Isotope Effects on Trapped-Electron-Mode Driven Turbulence and Zonal Flows in Helical and Tokamak Plasmas

Motoki Nakata,[*] Masanori Nunami, and Hideo Sugama

National Institute for Fusion Science, National Institutes of Natural Sciences, Toki 509-5292, Japan
The Graduate University for Advanced Studies, Toki 509-5292, Japan

Tomo-Hiko Watanabe

Nagoya University, Nagoya 464-8602, Japan

Impacts of isotope ion mass on trapped-electron-mode (TEM)-driven turbulence and zonal flows in magnetically confined fusion plasmas are investigated. Gyrokinetic simulations of TEM-driven turbulence in three-dimensional magnetic configuration of helical plasmas with hydrogen isotope ions and real-mass kinetic electrons are realized for the first time, and the linear and the nonlinear nature of the isotope and collisional effects on the turbulent transport and zonal-flow generation are clarified. It is newly found that combined effects of the collisional TEM stabilization by the isotope ions and the associated increase in the impacts of the steady zonal flows at the near-marginal linear stability lead to the significant transport reduction with the opposite ion mass dependence in comparison to the conventional gyro-Bohm scaling. The universal nature of the isotope effects on the TEM-driven turbulence and zonal flows is verified for a wide variety of toroidal plasmas, e.g., axisymmetric tokamak and non-axisymmetric helical or stellarator systems.

Turbulent transport and zonal-flow generation [1,2] are the universal physics in the drift-wave turbulence system in magnetized plasmas, and microinstabilities such as ion temperature gradient (ITG) modes and trapped electron modes (TEM) are typical causes of the turbulent transport to determine the confinement of the energy, particle, and momentum in magnetically confined toroidal plasmas [3]. Impacts of the isotope ion mass in hydrogen (H), deuterium (D), and tritium (T) on the energy confinement [4–8] and on the fluctuation characteristics [9,10] have been long-standing issues for several decades in plasma and fusion research, despite the broad interest and the importance for realizing sustainable fusion plasmas, which is one of the largest scientific challenges.

A simple theoretical evaluation of the turbulent diffusivity $\chi_{\text{turb.}}$ by the mixing-length diffusivity $\chi_{(\text{ML})}$ predicts a decrease of the energy confinement time τ_E ($\sim a^2/\chi_{\text{turb.}}$) due to the so-called gyro-Bohm scaling, indicating the isotope ion mass dependence of $\sqrt{A_i}$ in the mixing-length diffusivity, i.e., $\chi_{(\text{ML})} \sim (\gamma/k_{\perp}^2) \propto (\sqrt{A_i}/Z_i^2)\chi_{\text{GB(H)}}$ (γ: the growth rate of microinstability, $k_{\perp}$: the wave number, A_i: the mass number of ion species i, Z_i: the charge number, $\chi_{\text{GB(H)}}$: gyro-Bohm diffusivity for hydrogen ion). However, many experimental studies in tokamak devices such as ASDEX [4], JET [5], and JT-60U [6,7] have shown, more or less, the opposite isotope mass dependence, leading to improved energy confinement, e.g., $\tau_E \propto A_i^{0.5}$, depending on the heating and profile conditions. In stellarator devices, a slightly moderate dependence of $\tau_E \propto A_i^{0.2\pm0.15}$ has been observed in high-T_e/T_i

discharges with the electron-cyclotron resonance heating (ECRH) [8]. Also, some influences on the long-range turbulence correlation in the toroidal direction, which is regarded as a proxy of the zonal flow, have been observed [9,10]. The first-principle-based multispecies gyrokinetic simulations with isotope ions are powerful approaches to establishing theoretical understanding of the underlying physical mechanisms, as well as further investigations of the isotope effects by forthcoming hydrogen or deuterium experiments in, e.g., Large Helical Device (LHD), Wendelstein 7-X (W7-X), JT-60SA, and ITER.

So far much effort has been devoted to theoretical and numerical studies on the ITG-driven turbulent transport and the zonal-flow generation, based on the gyrokinetic model. In particular, several recent works have addressed the isotope effects on the ITG-dominated turbulence in tokamak plasmas [11,12]. However, the simulation results indicate a slight deviation from the gyro-Bohm mass dependence of the turbulent transport level, depending on the impurity species and the profile gradient regime, and did not reproduce the experimental tendency of $\chi_{\text{turb.}} \propto A_i^{\alpha}$, $\alpha < 0$. On the other hand, for the non-axisymmetric plasmas, such as LHD and W7-X, it has been found that the three-dimensional nature of the magnetic field leads to the isotope and/or global effects on the turbulent transport and the zonal-flow generation through the coupling with the equilibrium radial electric field [13–16]. The roles of the equilibrium radial electric field in the enhancement of zonal flows have also been investigated in several stellarator experiments [17,18].

In addition to the ITG modes, the TEM is often desta-bilized in a wide variety of toroidal plasmas [19] with high density gradients and/or electron temperature gradients, and the TEM-driven turbulent transport is another important transport channel in burning plasmas with the strong electron heating by the α particles. More recent gyrokinetic validation studies have identified a TEM-dominated state in the outer-core region of the L-mode plasmas [20,21]. Also, the impact of the TEM on the pedestal-top region has been found in the global simulation [22]. The fundamental properties of the collisionless TEM instability and the turbulent transport, including the impact of the zonal flow, have been investigated by analytic [23] and numerical [24–26] studies. As for the isotope effects on the TEM, although there are several linear analyses based on fluid [27] and kinetic [28,29] models, the nonlinear behavior, including the zonal-flow generation, has not been fully understood yet.

In this Letter, the isotope ion mass impacts on the TEM-driven turbulence and zonal flows in helical and tokamak plasmas are explored by using gyrokinetic simulations with real-mass kinetic electrons and the finite collisions. It is, for the first time, elucidated that the linear TEM stabilization by the isotope ions and the associated increase of the zonal-flow impact lead to the transport reduction distinct from the conventional gyro-Bohm mass dependence.

The linear and nonlinear analyses are carried out by an electromagnetic gyrokinetic Vlasov code GKV [30,31] with multiple-particle-species treatment [32] and realistic MHD equilibria in tokamak and helical plasmas. The time evolution of perturbed gyrocenter distribution functions $\delta f_s^{(g)}$ ("s" denotes the particle species) in the five-dimensional phase space $(x, y, z, v_{\parallel}, \mu)$ is numerically solved under a fixed equilibrium with the local Maxwellian F_{Ms}, where the so-called fluxtube coordinates of $x = a(\rho - \rho_0)$, $y = [a\rho_0/q(\rho_0)][q(\rho)\theta - \zeta]$, and $z = \theta$ are used (q: the safety factor, a: the plasma minor radius). Both the electrostatic ($\delta\phi_{k_\perp}$) and electromagnetic ($\delta A_{\parallel k}$) fluctuations in the wave number space with $k_\perp = k_x\nabla x + k_y\nabla y$ are treated in GKV simulations, but we focus on the low-β plasmas so that the magnetic fluctuation is quite small. Collisional effects are introduced in terms of an Lenard-Bernstein type linearized collision operator $\mathcal{C}_s$. The normalized collision frequency is defined as $\nu_{ss'}^* = qR_{ax}\tau_{ss'}^{-1}/(\sqrt{2}\varepsilon^{3/2}v_{ts})$, with the characteristic collision time $\tau_{ss'}$, the inverse aspect ratio ε, and the thermal speed $v_{ts} = (T_s/m_s)^{1/2}$. The scale lengths of the logarithmic gradients for the density and temperature are given by R_{ax}/L_{n_s} and R_{ax}/L_{T_s}, respectively. More detailed descriptions for the simulation model and the technical terms are given in, e.g., Refs. [28] and [33]. It should be stressed that a good prediction capability for the ion and electron energy fluxes has been confirmed in the validation study against the actual JT-60U tokamak [20] and LHD experiments [34].
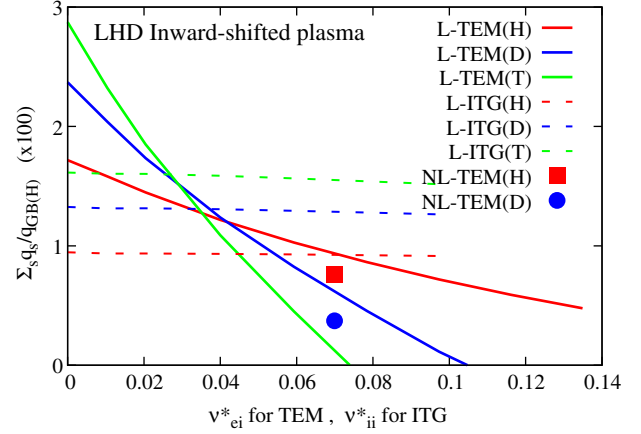

FIG. 1. Collisionality dependence of the radial heat flux $\sum_{s=i,e} q_s$ with the mixing-length diffusivity $\gamma/k_\perp^2$ for the linear TEM (L-TEM) and ITG (L-ITG) modes in LHD inward-shifted H, D, and T plasmas, where $k_x\rho_{ts} = 0$, $k_y\rho_{ts} = 0.4$ ($s = \{H, D, T\}$). For qualitative comparison, the nonlinear results from Fig. 2(a) are also displayed for the TEM case (NL-TEM).

In order to estimate the isotope ion mass impacts on the turbulent transport levels from the linear calculations, the collisionality dependencies of the radial heat flux, $\sum_{s=i,e} q_s = -n_s a\chi_s g^{\rho\rho} dT_s/d\rho$, for hydrogen (H), deu-terium (D), and tritium (T) plasmas are shown in Fig. 1, where $g^{\rho\rho}$ is the geometric factor, and the heat diffusivity χ_s is evaluated by the mixing-length diffusivity $\gamma/k_\perp^2$ for the fastest growing mode ($k_x\rho_{ts} = 0$, $k_y\rho_{ts} = 0.4$) in the linear calculations, and the hydrogen gyro-Bohm diffusivity $\chi_{GB(H)} = \rho_{tH}^2 v_{tH}/R_{ax}$, with the thermal gyrora-dius $\rho_{ts} = m_s v_{ts}/eB_{ax}$, is used as the unit. Here, we focus on the inward-shifted case in the LHD plasma with $R_{ax} = 3.60m$, $q(\rho_0) = 1.70$, $\hat{s}(\rho_0) = -0.96$, and $a\rho_0/R_{ax} = 0.082$, which shows the higher TEM growth rate compared with that in the standard configuration. The equilibrium profile parameters used here are $\{R_{ax}/L_{T_i} = 10, R_{ax}/L_{T_e} = 12, R_{ax}/L_n = 2, T_e/T_i = 1\}$ and $\{R_{ax}/L_{T_i} = 1, R_{ax}/L_{T_e} = 12, R_{ax}/L_n = 2, T_e/T_i = 2.5\}$ for ITG- and TEM-dominated cases, respectively, where these parameters are based on the high-temperature discharges in the actual LHD experiments, and the detailed linear spectra of the growth rate and mode frequency are given in Ref. [28]. For the cases in ITG modes (labeled by L-ITG in the figure) showing weak ν_{ii}^* dependence, we see that the linear results with the mixing-length diffusivity exhibit a gyro-Bohm ion mass dependence, i.e., $\gamma/k_\perp^2 \propto \sqrt{A_i}$. The similar $\sqrt{A_i}$ dependence is also found in the collisionless limit of TEM (labeled by L-TEM). This means that the TEM growth rate in the collisionless limit is scaled with the ion transit frequency of $\omega_{ti} = v_{ti}/q_0R_{ax}$. However, a different reduction tendency of the TEM cases depending on the isotope ion species is revealed in the finite collisionality regime, where the ion mass dependence in

the ratio of the electron-ion collision frequency to the ion transit frequency, i.e., $\nu_{ei}/\omega_{ti} \propto (m_i/m_e)^{1/2} \propto \sqrt{A_i}$, leads to stronger collisional stabilization for heavier isotope ions. Note also that the stabilization effect on ITG modes by the ion-ion collisions is almost independent of the ion mass, i.e., $\nu_{ii}/\omega_{ti} \propto m_i^0$. Then, the opposite ion mass dependence of A_i^α with $\alpha < 0$ appears for the TEM in a certain collisionality regime, i.e., $\nu_{ei}^* \geq 0.04$ in the present case. The reduction in the mixing-length diffusivity for the TEM through the collisional effects provides us with a useful qualitative basis to investigate the isotope impacts on the turbulent transport. For the comparison, which will be shown below, the nonlinear TEM results (labeled by NL-TEM) are also plotted in Fig. 1.

As for the linear zonal-flow response, earlier theoretical works show the weak isotope effects; i.e., the zonal-flow response kernel indicates no explicit mass dependence for the fixed $k_\perp \rho_{ti}$ [35], except for the cases with the equilibrium radial electric field [13–15]. Therefore, the isotope mass impacts on the nonlinear zonal-flow dynamics become more important.

Following the above linear analyses, we have performed massively parallel nonlinear TEM-driven turbulence simulations for the non-axisymmetric LHD plasma, where ~200 hours with 69,120 computation cores are required for a hydrogen case. The equilibrium parameter set for the TEM shown above is used, and $\nu_{ei}^* = 0.07$ is considered. We employ a number of grid points in $(x, y, z, v_\parallel, \mu)$ as $(256 \times 96 \times 320 \times 90 \times 24)$ for the ion and electron, where sufficiently large box sizes of $L_x = 147.3\rho_{tH}$ (or $k_{x(\min)}\rho_{tH} = 0.04265$) and $L_y = 148.1\rho_{tH}$ (or $k_{y(\min)}\rho_{tH} = 0.04243$) are taken for the comparison between H and D plasmas.

Nonlinear GKV simulation results on the time evolution of the turbulent radial heat flux $\sum_{s=i,e} q_s$, the turbulence energy $W_{\text{turb.}}$, and the zonal-flow energy W_{ZF} are shown in Figs. 2(a) and 2(b), where $W_{\text{turb.}}$ and W_{ZF} are defined as the nonzonal ($k_y \neq 0$) and the zonal ($k_y = 0$) components of $W_{\text{total}} = \langle \sum_{k_x,k_y} (e_s^2 n_s/2T_s)[1 - \Gamma_0(k_\perp^2 \rho_{ts}^2)]|\delta\phi_{\boldsymbol{k}_\perp}|^2 \rangle_z \simeq \langle \sum_{k_x,k_y} (n_i T_i/2)k_\perp^2 \rho_{ti}^2 (e^2|\delta\phi_{\boldsymbol{k}_\perp}|^2/T_i^2) \rangle_z$, with the field-line-averaging operator $\langle \cdots \rangle_z$. Also, the time evolution of the normalized entropy transfer from turbulence to zonal modes, $\sum_{s=i,e} T_s \mathcal{T}_s^{(\text{ZF})}/\sum_{s=i,e} q_s L_{T_s}^{-1}$, is shown in Fig. 2(c), where $\mathcal{T}_s^{(\text{ZF})}$ is regarded as a kinetic extension of the zonal-flow energy production due to the Reynolds stress (see Ref. [36] for the definitions) and should balance with the collisional dissipation for the zonal modes $\mathcal{D}_s^{(\text{ZF})}$ in the statistically steady turbulence state. Actually, the time averaged entropy balance relation of $\sum_{s=i,e} T_s \overline{\mathcal{T}_s^{(\text{ZF})}} + \sum_{s=i,e} T_s \overline{\mathcal{D}_s^{(\text{ZF})}} = 0$ (the overline means the time average) is accurately satisfied within a relative error of less than 10% in the present TEM turbulence simulations. As shown
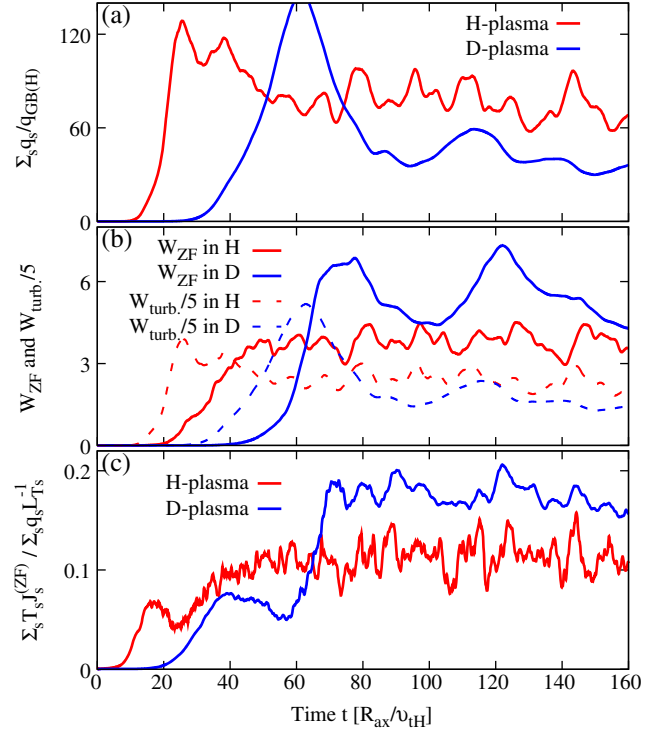

FIG. 2. Impacts of the hydrogen isotope mass on (a) turbulent heat fluxes normalized by the hydrogen gyro-Bohm unit ($\sum_s q_s/q_{\text{GB(H)}}$), (b) turbulence ($W_{\text{turb.}}$) and zonal-flow ($W_{\text{ZF}}$) energy, and (c) normalized entropy transfer to zonal flows ($\sum_s T_s \mathcal{T}_s^{(\text{ZF})}/\sum_s q_s L_{T_s}^{-1}$), where $s = \{i, e\}$, and $\nu_{ei}^* = 0.07$.

in Fig. 2(a) and also by symbols in Fig. 1, the turbulent transport level in the D plasma is lower than that in the H plasma, where the ratio of the mean turbulent transport level is evaluated as $[\sum_s q_s$ for D]$/[\sum_s q_s$ for H] $= 0.48$, which exhibits more significant reduction than that in the linear estimation with the ratio of 0.66. One also finds that the zonal-flow energy W_{ZF} increases in the D plasma in spite of the slight decrease of the turbulence energy $W_{\text{turb.}}$, where the zonal-flow enhancement characterized by the increase of the mean relative amplitude [14,34], $\overline{W_{\text{ZF}}/W_{\text{total}}}$ from 0.25 in H plasma to 0.39 in D plasma, is well correlated with the normalized entropy transfer shown in Fig. 2(c). The effective zonal-flow shearing rate defined by $\omega_{\text{ZF}}/\gamma_{\max}$ in the D plasma is more than twice as large as that in the H plasma, where $\omega_{\text{ZF}} = \langle|\partial_x v_{\text{ZF}}|\rangle_x$ means the shearing rate of the steady zonal flows, and $\langle \cdots \rangle_x$ denotes the spatial average in the radial (x) direction. As will be shown below, the increase of the zonal-flow impact at the near-marginal stability in the D plasma is induced by the stronger collisional stabilization of the TEM for heavier isotope ions.

Three dimensional spatial structures of the potential fluctuations are shown in Figs. 3(a)–3(d), where hydrogen and deuterium cases are displayed. For comparison, the results of Cyclone base case (CBC)-like tokamak TEM cases
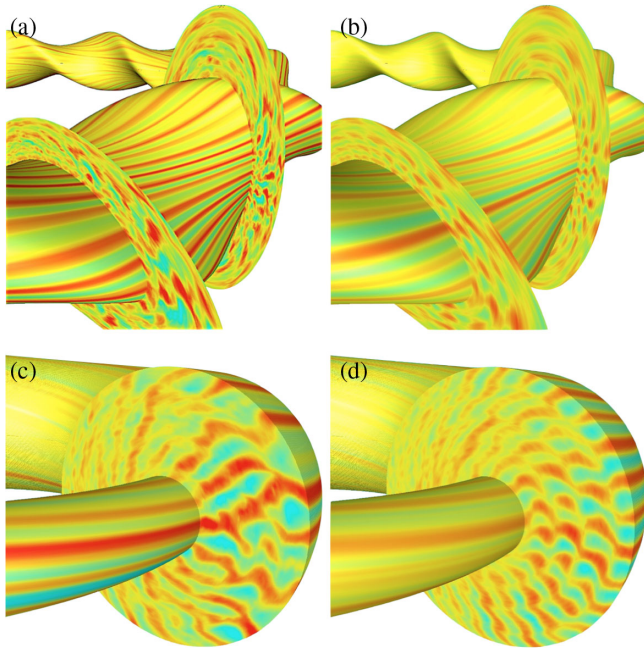
FIG. 3.   Spatial structures of the potential fluctuations in the TEM-driven turbulence for (a) LHD H, (b) LHD D, (c) CBC-like tokamak H, and (d) CBC-like tokamak D plasmas, where the simulation conditions of LHD and CBC tokamak cases correspond to those in Figs. 2 and 4(b) ($\nu_{ei}^* = 0.035$), respectively.
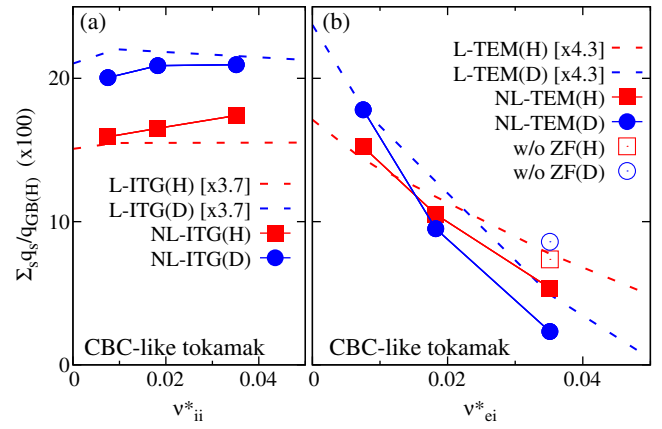

FIG. 4.   Collisionality dependence of the radial heat flux $\sum_s q_s$ for (a) ITG and (b) TEM cases in CBC-like tokamak plasmas, where the linear mixing-length (L) and the corresponding nonlinear (NL) results are plotted by dashed lines and line symbols, respectively. The linear results are uniformly scaled for qualitative comparison of profiles. NL-TEM cases without the zonal flow are also displayed by the open symbols.

(shown below) are also presented. We see more decorrelated structures in the radial direction with lower fluctuation amplitudes for both the helical and tokamak D plasmas with relatively stronger zonal-flow generation.

It should be stressed that since the collisional stabilization of the TEM shown in the present analyses is not particular for helical plasmas, the similar isotope effects on the turbulent transport and zonal flows are expected in tokamak plasmas as well. For verifying this, the nonlinear simulations for CBC-like tokamak plasmas are performed, where the equilibrium profile parameters of $\{R_{ax}/L_{T_i} = 8, R_{ax}/L_{T_e} = 8, R_{ax}/L_n = 3, T_e/T_i = 1\}$ and $\{R_{ax}/L_{T_i} = 1, R_{ax}/L_{T_e} = 8, R_{ax}/L_n = 3, T_e/T_i = 3\}$ are used for the ITG- and the TEM-dominated cases, respectively. The so-called $s-\alpha$ toroidal geometry, with $q(\rho_0) = 1.42$, $\hat{s}(\rho_0) = 0.8$ and $a\rho_0/R_{ax} = 0.18$, is considered. The GKV simulation results are summarized in Figs. 4(a) and 4(b), which are similar to those in Fig. 1. As is discussed in the above LHD case, the similar collisionality dependence is found for the linear tokamak ITG cases [labeled by L-ITG in Fig. 4(a)] with the gyro-Bohm mass dependence and for the linear tokamak TEM cases [labeled by L-TEM in Fig. 4(b)] with the opposite dependence on the isotope ion mass around $\nu_{ei}^* = 0.025$. It is also revealed that the ν_{ii}^* dependence of turbulent heat flux in the nonlinear ITG cases (labeled by NL-ITG) is qualitatively similar to that in the linear cases with the $\sqrt{A_i}$ dependence, where $\overline{W_{ZF}/W_{total}} \sim 0.2$ for all of the ITG cases. In contrast, as ν_{ei}^* increases, the

nonlinear TEM results (labeled by NL-TEM) show steeper decrease of the transport level in comparison to the linear cases, where $[\sum_s q_s \text{ for D}]/[\sum_s q_s \text{ for H}] = 0.43$ in the nonlinear TEM case for $\nu_{ei}^* = 0.035$, indicating more significant reduction than that in the linear estimation with the ratio of 0.63.

The transport reduction beyond the linear TEM stabilization is also attributed to the nonlinear turbulence suppression by the zonal flows as the TEM growth rate decreases towards the marginal stability with increasing ν_{ei}^*, as is similar to those in the near-marginal collisionless (or weakly collisional) ITG turbulence [37,38]. Indeed, Figs. 5(a) and 5(b) show the radial profiles of the long-time
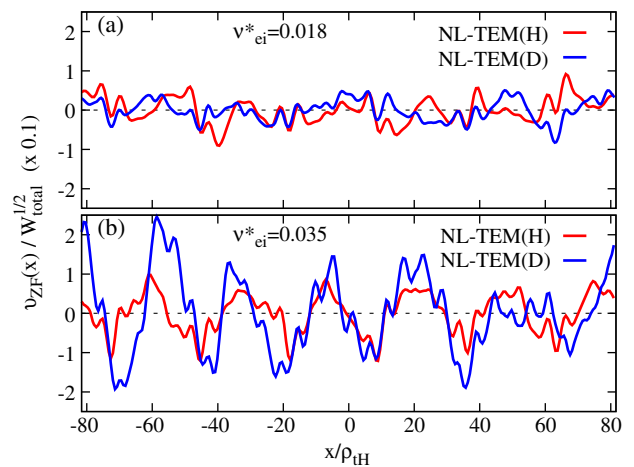

FIG. 5.   Radial profiles of TEM-driven zonal flows in CBC-like tokamak H and D plasmas for (a) $\nu_{ei}^* = 0.018$ and (b) $\nu_{ei}^* = 0.035$, where a larger relative amplitude of the steady zonal flow appears in D plasma with $\nu_{ei}^* = 0.035$ in comparison to the others.

averaged steady zonal flows in the TEM turbulence for H and D plasmas, where the cases with and without the transport reduction by the isotope effects (or correspondingly, $\nu_{ei}^* = 0.018$ and $\nu_{ei}^* = 0.035$) are compared. It is found that the relative amplitude of the steady zonal flows is enhanced in the near-marginal TEM stability [Fig. 5(b)], while the lower and comparable amplitudes are found in H and D plasmas with relatively higher TEM growth rates [Fig. 5(a)]. Also, the effective zonal-flow shearing ω_{ZF}/γ_{max} significantly increases from 0.76 in H plasma to 2.90 in D plasma with $\nu_{ei}^* = 0.035$, whereas it shows only slight increase from 0.44 to 0.63 for the cases with $\nu_{ei}^* = 0.018$. Although the relative amplitude of the TEM-driven zonal flows, e.g., $\overline{W_{ZF}/W_{total}} = 0.048$ in D plasma, with $\nu_{ei}^* = 0.035$, is much lower than that in the ITG cases, the numerical suppression of the zonal-flow components in the nonlinear simulation leads to more than 4 times the enhancement of the transport level [shown by the open symbols in Fig. 4(b)], which implies the crucial impact of the zonal flows in the near-marginal TEM stability. In the other cases with larger TEM growth rates, weaker zonal-flow impacts, which are pointed out in Ref. [25] for the collisionless TEM cases, have also been confirmed.

In summary, this Letter presents a critical mechanism of the isotope effects on the TEM instability, based on the systematic linear gyrokinetic analyses with finite collisions for both tokamak and helical plasmas. The ion mass dependence appearing in the ratio of electron-ion collision frequency to the ion transit frequency, which gives the characteristic frequency of the collisionless TEM, leads to the reduction in the TEM growth rate for the case with heavier isotope ions. The nonlinear gyrokinetic simulations have, for the first time, identified the significant transport reduction with the opposite ion mass dependence in comparison to the conventional gyro-Bohm scaling through the isotope effects of the collisional TEM stabilization and the steady zonal flows. It is noteworthy that the present isotope effects on the TEM are expected in a wide variety of toroidal plasmas, including tokamak and helical or stellarator plasmas, particularly for the outer-core and/or pedestal-top region with large density and/or electron-temperature gradients. In non-axisymmetric plasmas, the equilibrium radial electric field, which is ignored here, gives rise to an additional isotope effect on the zonal-flow enhancement [13–15,17,18]. In order to verify the present isotope mass effects, we need a precise setup of the fluctuation measurements and profile control to complement the previous experimental results. It should be stressed, though, that the reduction of the TEM-driven turbulent transport predicted here is qualitatively consistent with the experimental observations in ASDEX L-mode plasmas with $\tau_E \propto A_i^{0.5}$, where the increase of τ_E by the isotope effect becomes more pronounced in a higher electron density regime [4]. The forthcoming hydrogen or deuterium experiments in stellarator and tokamak devices, such as LHD, W7-X, and JT-60SA, are capable of investigating the isotope mass effects quantitatively, and our gyrokinetic analyses provide a possible operation scenario with the improved confinement.

---

*nakata.motoki@nifs.ac.jp

[1] Z. Lin *et al.*, Science **281**, 1835 (1998).

[2] A. Fujisawa *et al.*, Phys. Rev. Lett. **93**, 165002 (2004).

[3] W. Horton, Rev. Mod. Phys. **71**, 735 (1999).

[4] M. Bessenrodt-Weberpals *et al.*, Nucl. Fusion **33**, 1205 (1993).

[5] J. G. Cordey *et al.*, Nucl. Fusion **39**, 301 (1999).

[6] H. Urano, T. Takizuka, M. Kikuchi, T. Nakano, N. Hayashi, N. Oyama, and Y. Kamada, Phys. Rev. Lett. **109**, 125001 (2012).

[7] H. Urano, T. Takizuka, N. Aiba, M. Kikuchi, T. Nakano, T. Fujita, N. Oyama, Y. Kamada, and N. Hayashi, Nucl. Fusion **53**, 083003 (2013).

[8] U. Stroth *et al.*, Phys. Scr. **51**, 655 (1995).

[9] Y. Xu, C. Hidalgo, I. Shesterikov, A. Kramer-Flecken, S. Zoletnik, M. VanSchoor, and M. Vergote (the TEXTOR Team Collaboration), Phys. Rev. Lett. **110**, 265005 (2013).

[10] B. Liu, M. A. Pedrosa, B.Ph. van Milligen, C. Hidalgo, C. Silva, F. L. Tabarés, B. Zurro, K. J. McCarthy, A. Cappa, and M. Liniers, Nucl. Fusion **55**, 112002 (2015).

[11] I. Pusztai, J. Candy, and P. Gohil, Phys. Plasmas **18**, 122501 (2011).

[12] A. Bustos, A. B.Navarro, T. Görler, F. Jenko, and C. Hidalgo, Phys. Plasmas **22**, 012305 (2015).

[13] H. Sugama, and T.-H. Watanabe, Phys. Plasmas **16**, 056101 (2009).

[14] T.-H. Watanabe, H. Sugama, and M. Nunami, Nucl. Fusion **51**, 123003 (2011).

[15] A. Mishchenko, and R. Kleiber, Phys. Plasmas **19**, 072316 (2012).

[16] P. Xanthopoulos, G. G. Plunk, A. Zocco, and P. Helander, Phys. Rev. X **6**, 021033 (2016).

[17] M. A. Pedrosa, C. Silva, C. Hidalgo, B. A. Carreras, R. O. Orozco, and D. Carralero (TJ-II team Collaboration), Phys. Rev. Lett. **100**, 215003 (2008).

[18] R. S. Wilcox, B.Ph. van Milligen, C. Hidalgo, D. T. Anderson, J. N. Talmadge, F. S.B Anderson, and M. Ramisch, Nucl. Fusion **51**, 083048 (2011).

[19] P. Helander *et al.*, Plasma Phys. Controlled Fusion **54**, 124009 (2012).

[20] M. Nakata, M. Honda, M. Yoshida, H. Urano, M. Nunami, S. Maeyama, T.-H. Watanabe, and H. Sugama, Nucl. Fusion **56**, 086010 (2016).

[21] D. Told, F. Jenko, T. Görler, F. J. Casson, and E. Fable, Phys. Plasmas **20,** 122312 (2013).

[22] D. P. Fulton, Z. Lin, I. Holod, and Y. Xiao, Phys. Plasmas **21,** 042110 (2014).

[23] J. H. E. Proll, P. Helander, J. W. Connor, and G. G. Plunk, Phys. Rev. Lett. **108,** 245002 (2012).

[24] F. Merz and F. Jenko, Phys. Rev. Lett. **100,** 035005 (2008).

[25] J. Lang, S. E. Parker, and Y. Chen, Phys. Plasmas **15,** 055907 (2008).

[26] J. H. E. Proll, H. E. Mynick, P. Xanthopoulos, S. A. Lazerson, and B. J. Faber, Plasma Phys. Controlled Fusion **58,** 012006 (2016).

[27] M. Z. Tokar, D. Kalupin, and B. Unterberg, Phys. Rev. Lett. **92,** 215001 (2004).

[28] M. Nakata, M. Nunami, H. Sugama, and T.-H. Watanabe, Plasma Phys. Controlled Fusion **58,** 074008 (2016).

[29] Y. Idomura, J. Comput. Phys. **313,** 511 (2016).

[30] T.-H Watanabe, and H. Sugama, Nucl. Fusion **46,** 24 (2006).

[31] T.-H. Watanabe, H. Sugama, and S. Ferrando-Margalet, Phys. Rev. Lett. **100,** 195002 (2008).

[32] M. Nakata, M. Nunami, T.-H. Watanabe, and H. Sugama, Comput. Phys. Commun. **197,** 61 (2015).

[33] M. Nakata, A. Matsuyama, N. Aiba, S. Maeyama, M. Nunami, and T.-H. Watanabe, Plasma Fusion Res. **9,** 1403029 (2014).

[34] M. Nunami, T.-H. Watanabe, and H. Sugama, Phys. Plasmas **20,** 092307 (2013).

[35] H. Sugama, and T.-H. Watanabe, Phys. Plasmas **13,** 012501 (2006).

[36] M. Nakata, T.-H. Watanabe, and H. Sugama, Phys. Plasmas **19,** 022303 (2012).

[37] B. N. Rogers, W. Dorland, and M. Kotschenreuther, Phys. Rev. Lett. **85,** 5336 (2000).

[38] M. Nakata, and Y. Idomura, Nucl. Fusion **53,** 113039 (2013).